Microbes and Infection xxx (xxxx) 105337

Contents lists available at ScienceDirect

Microbes and Infection

journal homepage: www.elsevier.com/locate/micinf

Original article

Systemic inflammatory Th1 cytokines during *Trypanosoma cruzi* infection disrupt the typical anatomical cell distribution and phenotypic/functional characteristics of various cell subsets within the thymus

Maria Estefania Viano [a], Natalia Soledad Baez [a], Constanza Savid-Frontera [a], Eliana Ruth Baigorrí [a], Brenda Dinatale [b], Maria Florencia Pacini [b], Camila Bulfoni Balbi [b], Florencia Belén Gonzalez [b], Laura Fozzatti [a], Nicolas Leonel Lidón [a], Howard A. Young [d], Deborah L. Hodge [d], Fabio Cerban [a], Cinthia Carolina Stempin [a, 1], Ana Rosa Pérez [b, c, 1], Maria Cecilia Rodriguez-Galán [a, *]

[a] *Inmunología, CIBICI-CONICET, Facultad de Ciencias Químicas, Universidad Nacional de Córdoba, Argentina*
[b] *Instituto de Inmunología Clínica y Experimental de Rosario (IDICER CONICET-UNR), Argentina*
[c] *Centro de Investigación y Producción de Reactivos Biológicos (CIPREB), Facultad de Cs. Médicas de la Universidad Nacional de Rosario (UNR), Argentina*
[d] *Cancer and Inflammation Program, Center for Cancer Research, National Cancer Institute, Frederick MD 21702-1201, USA*

ARTICLE INFO

Article history:
Received 13 February 2024
Accepted 9 April 2024

Keywords:
Thymus
Candida albicans
Trypanosoma cruzi
IL-12
IL-18
IFNγ

ABSTRACT

The thymus plays a crucial role in T cell differentiation, a complex process influenced by various factors such as antigens, the microenvironment and thymic architecture. The way the thymus resolves infections is critical, as chronic persistence of microbes or inflammatory mediators can obstruct the differentiation.

Here, we illustrate that following inflammatory T helper 1 infectious processes like those caused by *Candida albicans* or *Trypanosoma cruzi*, single positive thymocytes adopt a mature phenotype. Further investigations focused on *T. cruzi* infection, reveal a substantial existence of $CD44^+$ cells in both the cortical and medullary areas of the thymus at the onset of infection. This disturbance coincides with heightened interferon gamma (IFNγ) production by thymocytes and an increased cytotoxic capacity against *T. cruzi*-infected macrophages. Additionally, we observe a reduced exportation capacity in *T. cruzi*-infected mice. Some alterations can be reversed in IFNγ knockout mice (KO). Notably, the majority of these effects can be replicated by systemic expression of interleukin (IL)-12 + IL-18, underlining the predominantly inflammatory rather than pathogen-specific nature of these phenomena.

Understanding the mechanisms through which systemic inflammation disrupts normal T cell development, as well as subsequent T cell exportation to secondary lymphoid organs (SLO) is pivotal for comprehending susceptibility to diseases in different pathological scenarios.

The thymus is a primary immune organ where the development of several types of lymphocytes take place [1,2] as natural killer T (NKT) cells, regulatory T cells (Tregs), mucosal-associated invariant T (MAIT) cells, and, more recently, innate $CD8^+$ T cells [1–3].

Under steady-state conditions, the integrity of the thymic microenvironment is indispensable for proper T cell development. Alterations in the cytokine milieu surrounding differentiating cells are critical to prevent disruptions in T cell ontogeny. In various pathological scenarios, such as infections, changes in soluble factors or antigens within the thymus may be responsible for deviations from normal T cell differentiation [3–5].

Changes in the thymic microenvironment can arise from two distinct scenarios: 1) Locally, through the direct infection of the thymus by various microorganisms [5] or 2) Systemically, due to the influence of glucocorticoids or inflammatory mediators produced by infections or inflammatory processes occurring elsewhere [3–5]. In either case, both situations are capable of disrupting the typical functionality of the thymus, potentially leading to alterations in the nature and status of the cells exported to SLO.

Multitude of pathogens are capable of infecting the thymus leading to thymic atrophy, alterations in tissue architecture and extracellular matrix, induction of pathogen-specific immune tolerance, release of autoreactive double negative (DN) or double positive (DP) thymocytes, and even disturbances in the normal development of thymocytes [5].

Prior research conducted in our laboratory has shown that systemic Th1 inflammatory or infection processes can disrupt the typical functionality and cellular composition of the thymus. Under these conditions, our laboratory has reported that not only can mature peripheral T

* Corresponding author. Inmunología. CIBICI-CONICET. Facultad de Ciencias Químicas. Universidad Nacional de Córdoba. Argentina. Fax: 54 351 4333048.
E-mail address: maria.rodriguez.galan@unc.edu.ar (M.C. Rodriguez-Galán).

[1] Contributed equally.

https://doi.org/10.1016/j.micinf.2024.105337
1286-4579/© 20XX

cells enter the thymus [6], but also the composition of conventional single-positive (SP) $CD8^+$ thymocytes (SP8) is altered. We have observed a substantial increase in innate memory $CD8^+$ T cells within the thymus following both intraperitoneal *Trypanosoma cruzi* infection **and** systemic expression of IL-12 + IL-18[3]. In this work, we aimed to analyze both the local modifications induced within the thymus, as well as the behavior of T cells exported to SLO during *T. cruzi* infection. In this context, our hypothesis is that systemic and local Th1 cytokines are triggered after these inflammatory/infectious processes, especially IFNγ, leading to changes in the thymic biology/structure. Moreover, we believe that these effects are primarily mediated by the inflammatory mediators themselves, rather than solely by the pathogens.

1. Materials and methods

1.1. Mice

Studies used 6–10 week old female and male WT C57BL/6, and IFNγ KO mice maintained under specific pathogen-free conditions.

The experimental protocols were approved by the Institutional Animal Care and Use Committee of Centro de Investigaciones en Bioquímica Clínica e Inmunología (CIBICI), Consejo Nacional de Investigaciones Científicas y Técnicas (CONICET). Our animal facility has obtained NIH animal welfare assurance (assurance no. A5802-01, Office of Laboratory Animal Welfare, NIH, Bethesda, MD, USA).

1.2. C. albicans and T. cruzi infections

T. cruzi trypomastigotes (Tulahuen) were maintained by serial passages in WT BALB/c mice. Mice used in experimental designs (C57BL/6) were intraperitoneal (i.p) infected with 5×10^5 trypomastigotes from *T. cruzi* diluted in PBS. Mice were euthanized between days 14–16 post-infection.

Yeast cells of *Candida albicans* were grown on Sabouraud glucose agar (Britania, Argentina) slopes at 28 °C and maintained by weekly subculture. B6 mice were i.p. injected with 3×10^7 viable yeast diluted in PBS. Mice were sacrificed 5 days after the infection.

1.3. Hydrodynamic cDNA injections

The hydrodynamic gene transfer procedure was described previously by our laboratory [3,6–11]. The designated amount of each DNA was dissolved in 1.6 mL of sterile 0.9% sodium chloride solution. Animals were separated into two groups and tail vein injected with control and test group in less than 8 s. The control group was injected with 15 μg of ORF empty vector control. The test group received murine IL-12 + IL-18 cDNAs expressing IL-12 and IL-18 proteins, respectively. Specifically, 1 μg of IL-12 cDNA (pscIL-12, p40-p35 fusion gene), with backbone from pcDNA3.11, CMV enhancer and promoter; SV40 intron; p35, mouse IL-12 p35 subunit; p40, mouse IL-12 p40 subunit as previously described [12]), 10 μg of IL-18 cDNA (pDEF pro-IL18) expression plasmid pcDEF/CMV driven by CMV promoter and human elongation factor-1 enhancer.

1.4. Peritoneal macrophages (PM)

C57BL/6 mice underwent intraperitoneal infection as described previously, then normal PM were obtained by several peritoneal washes by using PBS supplemented with 3% FBS (Natocor, Argentina). Non-infected animals were processed in parallel as control.

1.5. T. cruzi in-vitro Infection and co-culture experiments

Briefly, blood-derived trypomastigotes were used to infect Vero cell monolayers. After 7 days, supernatants were collected and stored at −80 °C. To perform *in vitro* infection of PM, cells were cultured for 3 h in a 24 well plate in complete medium to adhere. Cells were then washed three times and infected with *T. cruzi* (1:5, cell:parasites ratio). The day after, infected macrophages were co-cultured with previously stimulated phorbol 12-myristate 13-acetate (PMA)/Ionomycin (Cat#: P8139 and I9657 respectively, Sigma–Aldrich Chemical Co, EE. UU) thymocytes from control and *T. cruzi*-infected mice as effector cells (1:3, targets:effectors ratio) at 37 °C 5% CO2. Cells and supernatants were collected with intra-macrophage parasite counts performed by immunofluorescence (48 h after co-culture) or in the culture supernatants (72 h after co-culture).

1.6. Immunofluorescence staining

Parasite growth in PM was determined by counting the number of intracellular amastigotes using immunofluorescence. Coverslips were taken at 48 h after *T. cruzi* infection for immunofluorescence staining. Coverslips were washed in PBS and the cells were fixed for 40 min in 4% buffered formalin. Coverslips were washed in PBS and the cells were permeabilized with 1% Triton X-100 for 15 min. Coverslips were washed again in PBS, and cells were blocked with 1% BSA for 15 min. Slices were then stained with a serum from a chagasic patient. Subsequently, the samples were incubated with a FITC mouse anti-human IgG (Cat#: 555786, BD Pharmingen™). For nuclear staining, coverslips were incubated with 4′,6-diamino-2-phenylindole (DAPI), before being washed and incubated in mounting media FluorSave (Calbiochem®-Merck KGaA, Darmstadt, Germany) overnight.

For tissue immunofluorescence, thymi from C57BL/6 mice were collected and frozen over liquid nitrogen. Frozen sections with a thickness of 10 μm were cut, fixed for 10 min in cold acetone, left to dry at 25 °C and stored at −80 °C until use. Slides were hydrated in TRIS buffer and blocked for 30 min at 25 °C with 10% normal mouse serum in TRIS buffer. After blocking, slides were incubated with the corresponding primary Abs (rabbit anti mouse-CK-5 cat#: PRB-160P, Covance, and rat anti-mouse CD44 cat# 14-0441-82, ThermoFisher) for 90 min at 25 °C. Then, the samples were washed 3 times with PBS and subsequently incubated with the fluorochrome-labeled secondary Acs (AF488 anti-rabbit IgG cat#: A-21206 and AF594 anti-rat IgG cat# A-11007, ThermoFisher) for 60 min at room temperature. The preparations were washed and the cell nucleistained with DAPI. Finally, slides were mounted in FluorSave.

Slides were observed using an Olympus BX41 microscope (Olympus Corporation, Tokyo, Japan) and a Leica DMi8 microscope (Leica Microsystems). Images were processed with ImageJ software.

1.7. Flow cytometry and cell sorting

Phenotypic analysis of cells was performed by flow cytometry *ex vivo* at different days post infection as indicated previously. Samples were first washed with PBS and stained with Zombie Acqua Fixable Viability Kit (Biolegend) for 15 min at room temperature for exclusion of dead cells. Expression of different surface markers was assessed by staining with appropriate combinations of the following monoclonal antibodies (mAbs) for 30 min at 4 °C: APC-CY7-CD4 (clone: RM4-5, cat#: 100525, Biolegend), AF700-CD8 (clone: 53–6.7, cat#: 100729, Biolegend), FITC-CD44 (clone: IM7, Cat#: 11-0441-82, eBioscience), CD49d (clone: R1-2, cat#: 103618, Biolegend), PECy5-CD122 (clone: TM-β1, cat#: 123220, Biolegend), PE-NK1.1 (clone: PK136, cat#: 557391, BD bioscience), FITC-CD24 (clone: M1/69, cat#: 553261, BD Biosciences), APC-QA2 (clone: 695H1-9-9, cat#: 121714, Biolegend), PE-CCR5 (clone: C34-3448, cat#: 559923, BD Biosciences). Cells were washed twice with PBS and acquired on a BD LSR Fortessa X-20 cytometer (BD Biosciences).

To detect intracellular IFNγ expression, cells were cultured with PMA (50 ng/ml) and Ionomycin (1 μg/ml) for 4 h and 5 μg/ml

Brefeldin A (Sigma) was added during the last 3 h. Cells were then stained for surface markers, washed, and fixed with Cytofix/Cytoperm buffer (BD Pharmingen) for 30 min at 4 °C. Cells were washed with Perm Wash buffer (BD Pharmingen) and incubated with the PerCP-Cy5 anti-mouse IFNγ Ab (clone: XMG1.2, cat#: 560660, BD Pharmingen) or isotype-matched Ab (clone:MOPC-21 cat#:552834, BD Pharmingen) for 30 min at 4 °C. Following two washings, cells were analyzed in the flow cytometer.

For cell sorting, thymocytes were stained with monoclonal Abs and separated in a Becton Dickinson FACSAria II cytometer (BD Biosciences, San José CA, USA) as double negative (DN), double positive (DP), single positive $CD4^+$ (SP4), single positive $CD8^+$ (SP8), SP4 $CD44^{lo}$ or $CD44^{hi}$, SP8 $CD44^{lo}$ or $CD44^{hi}$, DP and NKT cells.

1.8. Cytokine quantification

Supernatants from cells treated *in vitro* were collected and assayed for IFNγ production by ELISA (cat#: 555138, BD-Pharmingen) according to the manufacturer's instructions.

1.9. Intrathymic injections and exportation experiments

B6 mice were intraperitoneally (i.p.) infected with 5×10^5 trypomastigotes from *T. cruzi*, which were diluted in PBS. Seven days post-infection, mice were anesthetized through i.p. injection of Ketamine (80–100 mg/kg)/Xylazine (10 mg/kg). An incision was then carefully made in the front neck of the animal to access the thymus without perforating the lung cavity. Subsequently, the thymic lobes were injected with 8 μl of eFluor 670 dye (cat#: 65–0840, eBioscience), which was diluted in physiological solution to a final concentration of 0.5 mM. Following the injection, the wounds of the mice were closed, and the animals were placed in a warm blanket to facilitate the recovery of their body temperature. Once fully awake and having completed their recovery, the mice were returned to their respective cages.

Five days after intrathymic injection, mice were sacrificed and thymus, spleen and a pool of inguinal and axillary lymph nodes (LNs) were obtained, in which, the frequency of $eFluor^+$ cells was evaluated.

1.10. mRNA analysis

Total RNA was extracted using a single-step phenol/chloroform extraction procedure (TRIzol; cat#: 15596026, Invitrogen Life Technologies). For the RNase protection assay (RPA), 5 μg of total cytoplasmic RNA were analyzed using the RiboQuan kits (BD Pharmingen) and [33P]UTP-labeled riboprobes as previously described [3,13].

1.11. Quantitative real-time RT-PCR

qRT-PCR was performed with a Quantitect SYBR Green RT-PCR kit (cat#: 204443, QIAGEN), according to the manufacturer's instructions and using a 7900HT Fast Real-Time PCR system (ABApplied Biosystems). The specific primer sequences used in RT/PCR are SIP1F: 5′AGCTCAGGGAACTTTGCGAG 3′ SIP1R: 5′GAGAAACAGCAGCCTCGCTC3′.

1.12. Adoptive transfer (AT) experiments

Thymi from control or IL-12 + IL-18 cDNA-injected mice were obtained and cell suspensions were prepared. Cells were counted and stained with 4 μM carboxyfluorescein succinimidyl ester (CFSE) dye. Approximately $5–6 \times 10^6$ total thymocytes were resuspended in 0.2 mL of sterile 0.9% sodium chloride solution and injected i.v into the B6 recipient. 1 week after adoptive transfer, the number of dividing cells was evaluated in spleen or LNs as the frequency of $CFSE^+$ cells.

1.13. Statistical analysis

Data were compared in all cases between each treated-mice group with its own control group. Results are expressed as means ± SEM. Data were analyzed using one-way analysis of variance (ANOVA) with a Bonferroni post-test to compare different columns ($p < 0.05$). In all cases, the assumptions of ANOVA (homogeneity of variance and normal distribution) were attained.

When indicated, significant differences were performed using Student's t test for paired or grouped samples. In all statistical analyses, $p < 0.05$ was considered to represent a significant difference between groups.

2. Results

We previously described that a certain number of mature T cells from SLO can enter the thymus when an inflammatory Th1 process results in high systemic levels of IL-12 and IL-18[6]. We have also described a similar effect during the acute phase of *T. cruzi* infection [6] where systemic levels of Th1 cytokines, IL-12 and IL-18, were reported [14,15]. As an additional support, we show in Supplementary Figure 1 that adoptively transferred splenocytes from *T. cruzi*-infected mice can enter the thymus and reside in the thymic medulla of resident *T. cruzi*-infected mice.

2.1. SP thymocytes adopt a mature phenotype after T. cruzi infection

Based on the work of Fink ***et al***. demonstrating that recent thymic emigrants (RTEs) within approximately three weeks of residence in SLO undergo a transition characterized by downregulation of CD24 and upregulation of QA2 surface markers [16]. **We** leveraged these two surface markers to assess the status of thymocytes in control mice following various inflammatory or infectious Th1 processes. As anticipated, Supplementary Figure 2 illustrates that control resident ($CD44^{lo}$) SP8 and SP4 thymocytes express the typical profile of immature T cells ($CD24^{hi}$ $QA2^{lo}$). Remarkably, we observed that under two distinct Th1 infectious processes, namely *C. albicans* and *T. cruzi* infections, this profile shifted toward a more mature phenotype ($CD24^{lo}$ $QA2^{hi}$). Furthermore, this transition to a mature state was also replicated through systemic exposure to the two inflammatory cytokines IL-12 and IL-18. In addition, the mature profile begins as early as the double-positive (DP) stage, especially marked by a significant upregulation of QA2.

2.2. Ectopic distribution of $CCR5^+IFN\gamma^+CD44^{hi}$ thymocytes after T. cruzi infection

We and other investigators has established that T cells with an activated/memory phenotype ($CD44^{hi}$) have a greater propensity to enter the thymus compared to naïve T cells [6,17,18]. To determine the specific anatomical localization of $CD44^{hi}$ cells, we collected thymus samples from both control and *T. cruzi*-infected mice and used immunofluorescence (IF) to examine the distribution of $CD44^+$ cells. In Fig. 1, we show in control mice, the majority of $CD44^+$ cells are located in the medulla, with few $CD44^+$ cells present in the cortex. Conversely, *T. cruzi*-infected mice exhibit a significant distribution of $CD44^+$ cells in both the thymic cortex and medulla. These findings indicate that during the acute phase of the infection, normal cellular distribution of the thymus is greatly disturbed, characterized by an abundance of $CD44^+$ cells distributed throughout the organ.

As previously indicated, the majority of alterations observed in the thymus following infections with *C. albicans* or *T. cruzi* can be replicated through systemic expression of the Th1 cytokines IL-12 and IL-18. Given the synergistic effect demonstrated by IL-12 + IL-18 in IFNγ production, we examined whether IFNγ could be locally generated in the thymus in response to systemic IL-12 + IL-18. Supplementary Figure 3

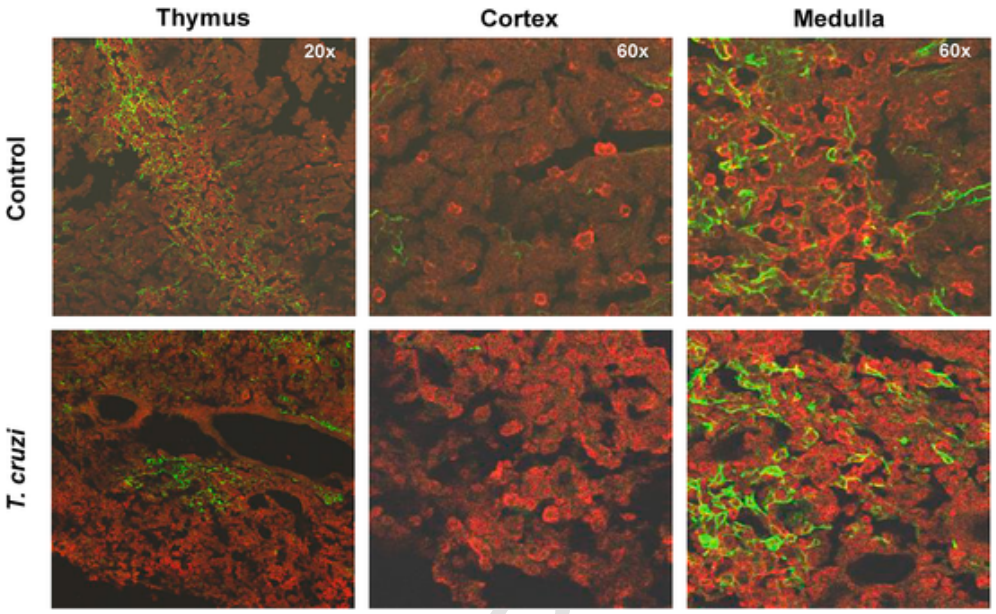

Fig. 1. Enrichment of CD44$^+$ cells in thymic cortical and medullary regions after *T. cruzi* infection. Thymi were harvested from control or *T. cruzi*-infected mice at 14–16 days post infection. Immunofluorescent staining of thymic medullary region by CK5 (green) and CD44 expression on thymocytes (red) are visualized in 10 μm thymic sections.

illustrates that while there is a rapid increase in IFNγ$^+$ cells in the spleen 24 h post-treatment, in the thymus, the response displays delayed kinetics, peaking at 4 days post-treatment. Furthermore, IFNγ RNA expression significantly escalates following *in vitro* IL-12 + IL-18 re-stimulation of thymocytes, with these cells being more prominent in *in vivo* IL-12 + IL-18 stimulated versus control mice (Fig. 2A). Similarly, at the protein level, we observed robust IFNγ production by thymocytes following either *in vitro* IL-12 + IL-18 (Fig. 2B) or αCD3-coated (Fig. 2C) stimulations, with consistently higher levels detected in thymocytes from *in vivo* IL-12 + IL-18-treated mice.

To examine this effect in an infectious context, we assessed IFNγ production by thymocytes from *T.cruzi*-infected mice. Fig. 3A illustrates

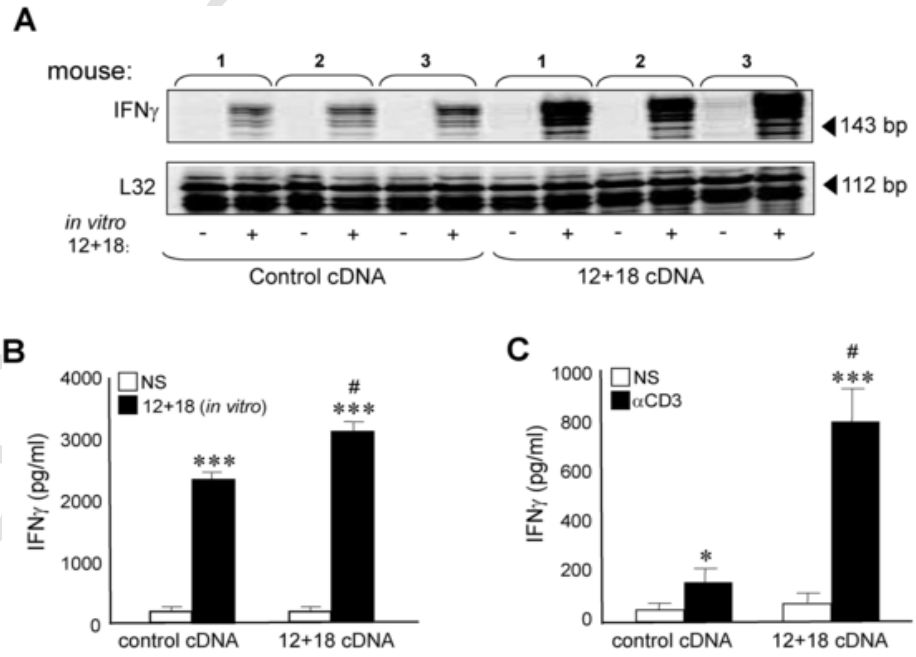

Fig. 2. Thymocytes from IL-12 + IL-18mice demonstrate elevated capacity to produce IFNγ after IL-12 + IL-18 or anti-CD3 *in vitro* stimulation. (A) IFNγ RNA expression of thymocytes isolated from control or IL-12 + IL-18 cDNA-*in vivo* treated mice were re-stimulated *in vitro* with recombinant mouse cytokines IL-12 and IL-18. IFNγ production was evaluated by ELISA in culture supernatants of thymocytes from control or **IL-12 + IL-18cDNA**-treated mice after *in vitro* (B) recombinant IL-12 + IL-18 or (C) anti-CD3 plate-coated antibody stimulation. Results are shown as mean ± SEM. Graphs are the pool of two independent experiments. NS = non-stimulated. *$p < 0.05$ or ***$p < 0.001$ in NS vs 12 + 18 or αCD3 *in vitro* stimulation (black vs white bars), #$p < 0.05$ Control cDNA vs 12 + 18-cDNA after 12 + 18 or αCD3 *in vitro* stimulation (black bars). The statistical test applied was a paired Student t test.

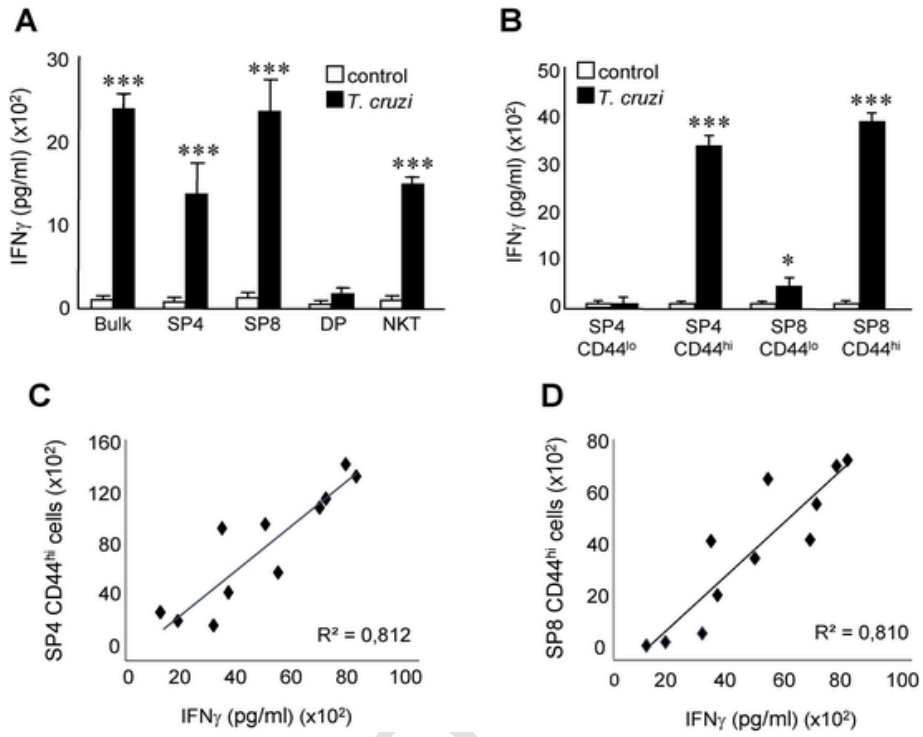

Fig. 3. IFNγ is produced by thymic NKT and CD44^{hi} SP4 and SP8 cells after *T. cruzi*-infection. (A) Total thymocytes (bulk) or different subpopulations were separated by cell sorting from control or *T. cruzi*-infected animals. Cells were cultured for 24 h in the presence of an anti-CD3 plate-coated antibody. IFNγ production was evaluated by ELISA in the culture supernatant. (B) CD44^{hi} or CD44^{lo} SP4 or SP8 thymocyte subpopulations from *T. cruzi*-infected mice were purified by cell sorting, cultured *in vitro* for 24 h in the presence of anti-CD3 plate-coated antibody and IFNγ production was determined in the culture supernatant by ELISA.
A linear correlation analysis between the absolute cell number of (C) SP4 CD44^{hi} or (D) SP8 CD44^{hi} and IFNγ production in thymus of *T. cruzi*-infected animals was performed. Results are shown as the mean ± SEM, the graph is representative of two independent experiments with similar results. Student t tests were performed and values of *$p < 0.05$ or ***$p < 0.001$ considered statistically significant. For C and D a linear regression analysis was applied and $R > 0.8$ was considered significant.

that the bulk population of thymocytes from *T. cruzi*-infected but not control mice results in elevated levels of IFNγ following αCD3 stimulation. This is similar to what was observed in IL-12 + IL-18-treated mice. Additionally, we sorted thymocytes at various maturation stages and found that IFNγ is produced by both SPs cells and NKT cells (Fig. 3A). Further analysis reveals that IFNγ is predominantly generated by CD44^{hi} SP thymocytes (Fig. 3B), with IFNγ levels positively correlating with the number of SP4 CD44^{hi} (Fig. 3C) or SP8 CD44^{hi} (Fig. 3D) cells in thymi following *T. cruzi* infection.

Thymocytes from *T. cruzi*-infected mice also acquired another Th1 marker, the chemokine receptor CCR5. Whether after systemic IL-12 + IL-18 expression (Supplementary Figure 4A) or *T. cruzi* infection (Supplementary Figure 4B), CCR5 RNA expression is elevated. Particularly, CCR5$^+$ cells are more abundant in CD44^{hi} than CD44^{lo} SP thymocytes after *T. cruzi* infection (Supplementary Figure 4C).

2.3. *Thymocytes from T. cruzi-infected mice acquire a cytotoxic profile and have reduced exportation to SLO*

In order to assess whether the Th1 profile adopted by thymocytes correlate with a functional profile, we evaluated the cytotoxic capacity of thymocytes residing in the thymi of animals infected with *T. cruzi*. We observed that the percentage of intracellular parasites in peritoneal macrophage-enriched cells is significantly lower when co-cultured with thymocytes from *T. cruzi*-infected animals compared to those from control animals (Fig. 4A and B). A similar result was observed when analyzing the number of parasites present in supernatants (Tpm) of the co-cultures (Fig. 4C).

To investigate the export capacity and phenotype of RTEs from control versus *T. cruzi*-infected mice, we conducted intrathymic injections with eFluor 660 dye (eF) on day 8 post-infection and evaluated eF$^+$ cells in SLO on day 14 post-infection (gate strategy in suppl. Figure 5). We observed a significant reduction in the frequency of both CD4$^+$ (Fig. 5A) and CD8$^+$ (Fig. 5B) RTEs in the lymph nodes and spleen of *T. cruzi*-infected mice. However, the diminution in the exportation of both CD4$^+$ or CD8$^+$ RTEs can be only seen in the spleen, while no such reduction is observed in the LNs (Fig. 5C and D). This data could be partially reproduced after adoptive transfer of CFSE$^+$ thymocytes from control or 12 + 18-treated mice where the percentage of CD8$^+$CFSE$^+$ T cells from IL-12 + IL-18-treated mice was significantly lower in both lymph nodes (Supplementary Figure 6A) and the spleen (Supplementary Figure 6B) compared to CD8$^+$CFSE$^+$ T cells from control mice.

The regulation of thymocyte egress primarily relies on the interplay between sphingosine 1-phosphate (S1P) and sphingosine 1-phosphate receptor-1 (S1PR1). The activation marker CD69, which increases in thymocytes during positive selection, exerts a negative influence on the surface expression of S1PR1 [19]. This prompted us to analyze whether the diminished thymic export observed in *T. cruzi*-infected mice could be attributed to alterations in the expression of CD69 and S1PR1 on SP4 and SP8 thymocytes.

Contrary to our expectations, our investigation revealed an upregulation of S1PR1 RNA expression in SP4 cells and no discernible modification in SP8 cells between control and *T. cruzi*-infected mice (Supplementary Figure 7A). Recognizing the heterogeneity within the SP4 and SP8 thymocyte populations, consisting of CD44^{lo} and CD44^{hi} cells, and considering the documented interaction between CD69 ex-

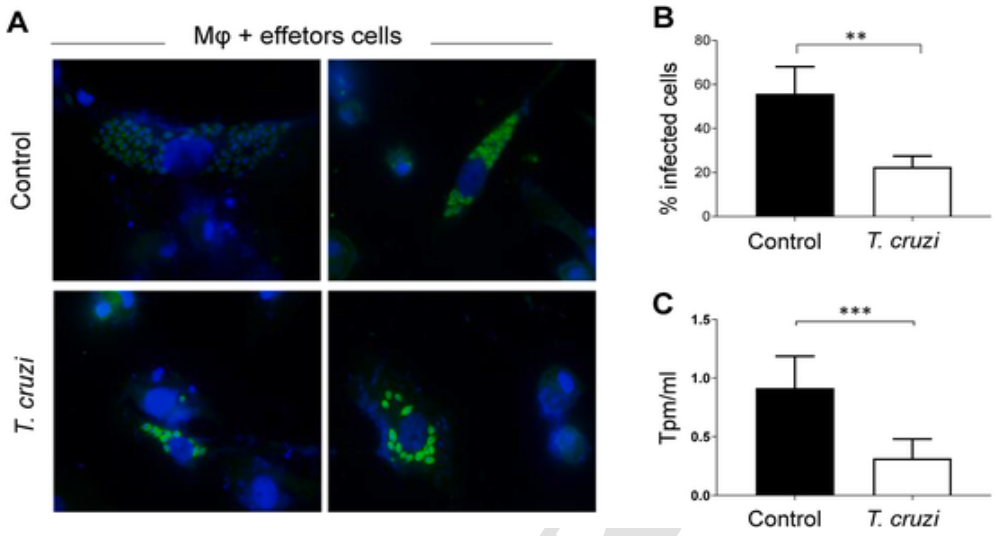

Fig. 4. Thymocytes from *T. cruzi*-infected mice have a high cytotoxic capacity against *T.cruzi*-infected macrophages. A bulk thymocytes population obtained from control or *T.cruzi*-infected mice (effectors) was co-cultured with peritoneal macrophages (PM) previously infected *in vitro* with *T. cruzi* (targets). Killing capacity was determined by (A–B) the number of parasites inside PM evaluated by immunofluorescence staining 48 h post-co-cultures and (C) the number of parasites in the culture supernatants (Tpm) 72 h after co-cultures. Nuclei are stained with DAPI and parasites are in green (FITC). The statistical test applied was a paired Student t test, *p < 0.05, **p < 0.01 or ***p < 0.001.

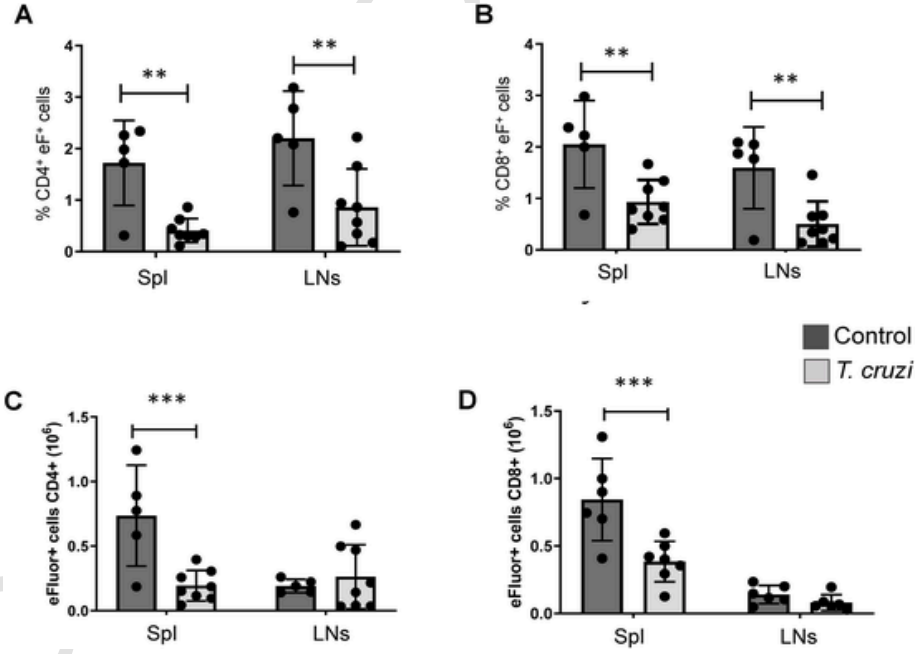

Fig. 5. A lower frequency of both CD4$^+$ and CD8$^+$ RTEs in SLO of *T. cruzi*-infected mice. Thymi of control or *T. cruzi*-infected mice were injected with 10 μl of eFluor660 dye (eF) at day 8 post-*T. cruzi* infection. **Five** days later (day 14 post-infection), mice were euthanized and thymi, LNs and spleen were harvested with frequency and absolute number of CD4$^+$ (A and C, respectively) or CD8$^+$ (B and D, respectively) eF$^+$ RTEs calculated by flow cytometry analysis. Statistical analysis of the percentage and absolute number of CD4$^+$ and CD8$^+$ RTEs in total eF$^+$ cells was performed by one way ANOVA, **p < 0.01 or ***p < 0.001.

pression and S1PR1 downregulation, we assessed CD69 expression on SP4 and SP8 thymocytes, distinguishing between CD44^{lo} and CD44^{hi} subsets.

Our findings unveil a significant downregulation of CD69 expression in SP4 CD44^{hi} cells from *T. cruzi*-infected mice compared to control counterparts, while the expression remains unchanged in SP4 CD44^{lo} cells between the two groups of mice (Supplementary Figure 7B). This disparity in CD69 expression inside the SP4 population may explain the heightened overall S1PR1 RNA expression in the bulk SP4 cell subset from *T. cruzi*-infected mice. Conversely, although SP8 CD44^{hi} cells downregulated S1PR1 expression in *T. cruzi*-infected mice, SP8 CD44^{lo} cells exhibited an upregulation in its expression in these mice. This dynamic could potentially contribute to a compensation that leads to similar S1PR1 transcript levels between control and *T. cruzi*-infected mice in the bulk SP8 population (Supplementary Fig. 7A and 7B).

2.4. Thymic involution and thymocyte phenotype are altered in IFNγ KO mice during T. cruzi infection

To explore whether induced thymic IFNγ production in *T. cruzi*-infected mice may underlie some of the observed changes in this study, we assessed parameters such as cellularity, thymic involution, percentage of SP cells and QA2/CD24 expression in the thymi of IFNγ KO mice compared to control WT mice following *T. cruzi* infection.

We describe here that all IFNγ KO mice succumb to infection by day 9–10, contrary to most WT mice that remain alive by days 14–16 post-infection. This observation led us to conduct a detailed analysis of various thymic features at this early time point in both WT and IFNγ KO mice.

The data presented in Fig. 6 illustrates that, at day 9–10 post *T. cruzi* infection (dpi), WT mice exhibit a partial reduction in thymic cellularity, consistent with our laboratory's previous findings [6]. In contrast, IFNγ KO mice display a more substantial loss in cellular content, indicative of severe thymic involution (Fig. 6A). Fig. 6B demonstrates that this effect is primarily attributable to the depletion of DP thymocytes, leading to an elevated proportion of SP4 and SP8 cells (Fig. 6C and D, respectively).

As reported earlier by our laboratory, the partial reduction in cellularity observed in WT mice correlates with an increase in SP CD44^{hi} cells [6]. However, this effect is notably absent in IFNγ KO mice (Fig. 6E and D). Concurrently, at this post-infection timeframe, alterations in QA2/CD24 expression are not discernible between control and *T. cruzi*-infected mice (Supplementary Figure 8).

3. Discussion

The thymus is a crucial primary lymphoid organ responsible for the differentiation of various T cell lineages. Thymic selection processes rely heavily on the surrounding environment and the architectural integrity of the thymus. Local infections in the thymus or the presence of inflammatory mediators during systemic infections can significantly modify these features [20]. While it was once believed to be an immune-privileged site, it is now evident that the thymus is susceptible to infection and plays a role in the development of immune responses [5]. In such pathological scenarios, the differentiation of pathogen-specific T cells may be disrupted, potentially reducing resistance to infections [5]. In this context, data presented here illustrate how systemic Th1 inflammatory processes, triggered by different pathogens, can influence the maturation stage of developing thymocytes. Moreover, our research provides valuable insights into how the anatomical distribution of cells and the composition of the thymus are altered following systemic *T. cruzi* infection. Furthermore, our study demonstrates that some of these effects can be replicated through the systemic induction of the inflammatory cytokines IL-12 and IL-18.

Prior research has shown that various microorganisms, such as bacteria, viruses, fungi, and parasites (including *T. cruzi*), have the capacity to directly infect the thymus [5,21]. This invasion can lead to significant impacts on the development of immature T cells, as emphasized in the review by Correia Neves laboratory [5].

Systemic *T. cruzi* infection induces thymus atrophy through the production of tumor necrosis factor alpha (TNFα) and corticosterone, as demonstrated in previous research [5,22]. Notably, we and others have previously shown that thymic atrophy progresses gradually in the days following infection [4,6]. We previously documented significant thymic alterations occurring between days 14–16 post-infection [3,6]. This phenomenon aligns with a pronounced accumulation of CD44^{hi} cells within the SP subset [3,6].

These memory-like cells results from both the entry of mature T cells from secondary lymphoid organs [6] and the transition towards the development of innate memory CD8^{+} cells among SP8 thymocytes [3]. Similarly, Morrot et al. have reported the existence of DP thymocytes exhibiting an activated/effector phenotype (CD44^{hi}) exclusively after *T. cruzi* infection [4]. In particular, our study reveals that during the acute phase of *T. cruzi* infection, CD44^{+} cells are highly abundant in both the thymic cortex and medulla along with phenotypically mature DP and SP thymocytes (CD24^{lo} QA2^{hi}). In this context, it has been documented that *T. cruzi* induces heightened deposition of fibronectin and laminin, accompanied by increased production of chemokine CXC ligand (CXCL) 12 and chemokine CC ligand (CCL)4 within the thymus [23,24]. Furthermore, during *T. cruzi* infection, there is an upregulation in the expression of CXCR4 and CCR5 on thymocytes, leading to enhanced intrathymic migration of DP cells [23,24]. Our observations indicate a notable augmentation in CCR5 expression in SP CD44^{hi} cells, which may partly explained the presence of CD44^{+} cells observed throughout the organ.

CD44^{hi} cells in the thymus not only disrupts the typical organ architecture but also, as we have shown, have the capacity to produce the inflammatory cytokine, IFNγ. Notably, this production is primarily attributed to SP4 and SP8 CD44^{hi} cells, highly enriched in the thymi of *T. cruzi*-infected mice. Intriguingly, similar results were observed following systemic expression of IL-12 and IL-18, suggesting that this effect may be driven more by systemic inflammatory conditions rather than by the pathogen itself. In this context, we have previously demonstrated that after systemic infection with Th1-driven pathogens like *C. albicans* or two strains of *T. cruzi* or following IL-12 + IL-18 expression, SP8 thymocytes alter developmentally towards an innate memory CD8^{+} phenotype [3]. This contrasts with the conventional SP8 development observed in control mice [3]. In summary, after *T. cruzi* infection, the thymus mimics an active immune tissue, featuring cells in the SP compartment exhibiting a mature Th1 activated/memory phenotype (QA2^{hi} CD24^{lo} CD44^{hi} CCR5^{+} IFNγ^{+}), along with a notable cytotoxic capacity to reduce the number of parasites in *T. cruzi*-infected macrophages.

Lymphocyte egress relies on S1PR1, whereas CD69 expression can impede S1P-mediated T cell exit from lymphoid tissues [19]. In our model, *T. cruzi*-infected mice exhibit a reduced exportation of SP4 and SP8 thymocytes to SLO. In other infectious processes, it has been previously reported that during thymic human immunodeficiency virus (HIV) or *Mycobacterium tuberculosis* infections, alterations in T cell output could be generated [25,26].

Our first conclusion was that the reduction in the exportation rate in SPs thymocytes does not directly correlate with RNA S1PR1 expression by these cell subsets. Given that SP4 in the thymus primarily consists of CD44^{lo} and CD44^{hi} cells, we investigated CD69 expression in these thymic populations using flow cytometry. Previous reports developed in co-expression experiments reveal that CD69 inhibits S1P1 chemotactic function and results in the downmodulation of S1P1 [19]. Consequently, the overall CD69 in SP bulk populations (CD44^{lo} + CD44^{hi} cells) correlate with S1PR1 expression in total SP4 and SP8 thymocytes. However, thymic cell exportation is a complex phenomenon where additional molecules may be involved, necessitating further investigation to comprehensively understand the reduced release of RTEs during *T. cruzi* infection. For instance, Cotta-de-Almeida reports that *T. cruzi* or *Plasmodium berghei* infection induce premature egress of DP thymocytes, data that do not align with our experiments showing undetectable S1PR1 in DP cells [23,27].

The cytokine milieu within the thymus is comprised of several cytokines, each playing distinct roles during T cell ontogeny [3,13,28]. Imbalances in this milieu could potentially lead to disruptions in normal T cell development and selection processes [3,29].

While numerous publications have highlighted the significance of type I and III interferons in thymic biology [30], there is a noticeable paucity of information concerning the role of IFNγ in the thymus despite the presence of various sources of this cytokine, such as thymic NKT1 cells, γδ T cells and innate CD8^{+} cells [3,31]. In this context, we investigated whether the IFNγ expression observed in the thymi of *T.*

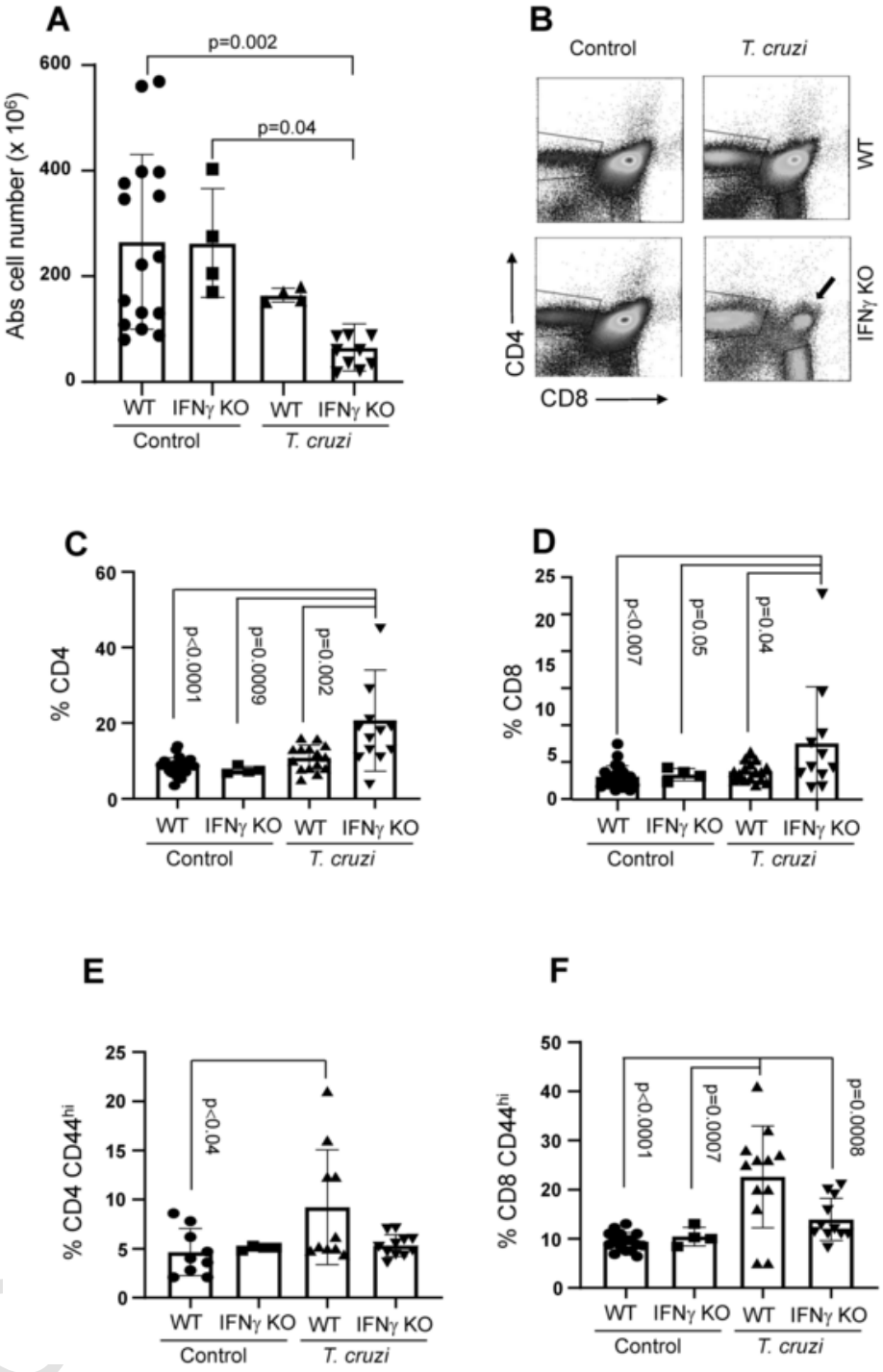

Fig. 6. IFNγ KO mice experience substantial loss of thymic cellularity and CD44^{hi} cells early after*T. cruzi* infection. Thymocytes from WT or IFNγ KO, control or 9–10 days post *T. cruzi*-infected mice were obtained. (A) The absolute number of cells was calculated by manual count with trypan blue. The frequency of SP4 and SP8 cells in WT or IFNγ KO mice was evaluated by using flow cytometry. (B) Representative dot plot of SP4 and SP8 cells in thymus from control and *T. cruzi*-infected mice from both strains. (C–D) Frequency of SP4 and SP8 cells. (E–F) Frequency of CD44^{+} cells in both SP4 and SP8 thymocytes evaluated by flow cytometry in both mice strains used, in control and *T. cruzi*-infected mice. One-way ANOVA was used for statistical analysis. Data are shown as the mean ± SEM, p values from control versus *T. cruzi*-infected in both WT and IFNγ KO mice are indicated in the figure.

cruzi-infected mice could contribute to some of the observed organ changes. For instance, we have previously reported that IL-12 + IL-18 *in vitro*-stimulated thymocytes induce IA-IE expression in thymic cortical and medullary epithelial cell lines in an IFNγ-dependent manner [13].

In this work, our findings indicate that in the absence of IFNγ, thymic atrophy is exacerbated, accompanied by a substantial loss of DP cells and an enrichment of SP cells at a significantly shorter time point than observed in WT *T. cruzi*-infected mice. Particularly noteworthy is the absence of the high abundance/recruitment of CD44^{+} cells, although the QA2/CD24 expression pattern remains unaltered. This data demonstrate that IFNγ may indeed play a role in the alterations ob-

served in the thymus following systemic infection with this parasitic pathogen.

In summary, our work provides evidence that, following Th1 systemic inflammatory/infectious processes, the thymus is sensitive to this non-physiological environment, resulting in both the influx of mature cells from SLO and local disturbances in the normal pathway of differentiation. The abnormal distribution of cells, especially $CD44^{hi}$ cells, in the thymic cortex and medulla of *T. cruzi*-infected mice may also interfere with the regular selection processes that ensure proper exportation and residence of T cells in secondary lymphoid organs.

Funding sources

This work was supported in part by the Intramural Research Program of the Center for Cancer Research, National Cancer Institute (NCI), Cancer Innovation Laboratory (CIL) USA, under grant No. 1ZIABC009283-36. The views expressed in this article are those of the authors and do not necessarily reflect the official policy or position of the Department of Health and Human Services, nor does mention of trade names, commercial products, or organizations imply endorsement by the United States Government.

This work was partially supported by Secretaría de Ciencia y Tecnología from Universidad Nacional de Córdoba (SECyT), Agencia Nacional de Promoción Científica y Tecnológica (ANPCyT), Fondo para la Investigación Científica y Tecnológica (FONCyT), and Consejo Nacional de Investigaciones Científicas y Técnicas (CONICET).

CRediT authorship contribution statement

Estefania Viano: Conceptualization, Data curation, Formal analysis, Investigation, Methodology, Visualization. **Natalia S. Baez:** Data curation, Investigation, Methodology. **Constanza Savid-Frontera:** Investigation, Methodology. **Eliana Baigorrí:** Investigation, Methodology. **Brenda Dinatale:** Methodology. **Maria Florencia Pacini:** Methodology. **Camila Bulfoni Balbi:** Methodology. **Florencia Belén Gonzalez:** Methodology. **Laura Fozzatti:** Methodology. **Nicolas L. Lidón:** Methodology. **Howard A. Young:** Funding acquisition, Writing – original draft. **Deborah Hodge:** Methodology, Writing – original draft, Writing – review & editing. **Fabio Cerban:** Methodology. **Cinthia Stempin:** Conceptualization, Formal analysis, Methodology, Visualization. **Ana Rosa Pérez:** Conceptualization, Data curation, Methodology, Visualization. **Maria Cecilia Rodriguez Galán:** Conceptualization, Data curation, Formal analysis, Funding acquisition, Investigation, Methodology, Project administration, Supervision, Validation, Visualization, Writing – original draft, Writing – review & editing.

Declaration of generative AI and AI-assisted technologies in the writing process

During the preparation of this work the author(s) used ChapGPT in order to improve the quality of the English grammar. After using this tool/service, the author(s) reviewed and edited the content as needed and take(s) full responsibility for the content of the publication.

Declaration of competing interest

All authors have agreed to the submission of this manuscript and declare that the research was conducted in the absence of any commercial or financial relationships that could be construed as a potential conflict of interest.

Acknowledgments

The authors thank Diego Luti, Victoria Blanco, Cecilia Noriega, Dr. Soledad Miro, Sergio Oms for animal care. Dr. Pilar Crespo and Dr. Paula Abadie for FACS technical support. Dr. Laura Gatica, Lic. Gabriela Furlan and Dr. Noelia Maldonado for cell culture support, Dr. Laura Gatica for histological technical support and Paula Icely for overall experimental technical assistance.

Appendix A. Supplementary data

Supplementary Figure 1. Mature cells from SLO enter the thymus of *T. cruzi*-infected mice. B6 mice were infected with *T. cruzi* and splenic cells suspensions obtained 14-day post-infection. Splenocyte suspensions were stained with eF dye and 4–8 x 10^6 cells were adoptively transferred (AT) to a group of recipient B6 *T. cruzi*-infected mice on the day 13 post-infection. Mice were sacrificed 24 h post AT and thymi were harvested and fixed in 4% paraformaildehyde. Histological sections were obtained (10 micron) using a cryostat and a subsequent immunofluorescence was performed. Shown in green (Alexa fluor 488 nm) are the Thymic Medullary Epithelial Cells (mTEC) labeled with an anti-CK5 antibody, in blue are the nuclei labeled with DAPI and in red are the transferred cells (eF^+).Supplementary Figure 2. Thymocytes acquire a mature-like phenotype after Th1 inflammatory/infectious conditions. Thymocytes from WT control or IL-12 + IL-18-treated (day 7), *C.albicans*- (day 7) or *T. cruzi*-infected (day 14-16) mice were obtained in the indicated time points post-treatment or infection. The expression of CD24 and QA2 was evaluated by flow cytometry in the DP, SP4 $CD44^{lo}$ and SP8 $CD44^{lo}$ resident thymocytes. One-way ANOVA was used for statistical analysis. Data are shown as the mean ± SEM, p values from Control versus IL-12 + IL-18-treated, *C.albicans*- or *T. cruzi*-infected mice are indicated in the figure.Supplementary Figure 3. IFNγ production is observed in thymus and spleen after systemic IL-12 + IL-18 expression. Thymi and spleens were harvested and cell suspensions obtained on day 7 post- hydrodynamic injection of control or IL12 + IL-18 cDNA plasmids. $IFN\gamma^+$ cells were analyzed by flow cytometry (top) and IFNγ RNA evaluated by RPA (bottom) from ex-vivo cultures at different days post injection (24, 48, 72 and 96 h). NS = not significant. Results are shown as mean ± SEM of three independent experiments. The statistical test applied was a paired Student t test and values of $*p < 0.05$ were considered statistically significant.Supplementary Figure 4. Expression of CCR5 is preferentially shown by SP4 and SP8 $CD44^{hi}$ thymocytes. (A) RNA was extracted from thymocytes isolated from animals injected with control or IL-12 + IL-18 cDNA expression plasmids up to day 4 post-treatment and assessed for CCR5 expression by RPA (mcR-5). (B) Thymocytes were isolated from control or *T. cruzi*-infected mice and assessed for CCR5 RNA expression by RT-PCR. (C) CCR5 expression was evaluated flow cytometry in $CD44^{lo}$ or $CD44^{hi}$ SP4 and SP8 thymocytes obtained from control or *T. cruzi*-infected mice. The statistical test applied was a paired Student t test. Results are shown as mean ± SEM, the graph is representative of 2-3 independent experiments with similar results. Values of $*p < 0.05$ were considered statistically significant.Supplementary Figure 5. Gating strategy for thymic exportation. Gating strategy to evaluate the thymic exportation of SP4 and SP8 thymocytes in control or *T. cruzi*-infected mice.Supplementary Figure 6. Reduced number of adoptively transferred SP4 and SP8 thymocytes from IL-12 + IL-18 cDNA-treated mice in SLO. Thymocytes from control or IL-12 + IL-18-cDNA injected mice were stained with 4 μM CFSE dye. Approximately 5-6 $\times 10^6$ total $CFSE^+$ thymocytes were injected i.v into B6 recipient mice. One week after adoptive transfer, the number of SP4 and SP8 $CFSE^+$ cells were evaluated in (A) LNs or (B) spleen by flow cytometry. The statistical test applied was a paired Student t test, $*p < 0.05$.Supplementary Figure 7. Correlation between CD69 and S1RP1 expression in SP4 and SP8 thymo-

cytes from *T.cruzi*-infected mice. (A) mRNA was extracted from sorted thymocytes from control and *T. cruzi*-infected mice. Thymocytes were stained with CD4 and CD8 antibodies to separate DN, DP, SP4 and SP8 populations and S1RP1 mRNA levels evaluated by qRT-PCR. ***$p < 0.001$, # not detectable. (B) CD69 expression was evaluated on SPs $CD44^{lo}$ and $CD44^{hi}$ thymocytes from control or *T. cruzi*-infected mice by conventional flow cytometry.Supplementary Figure 8. Lack of changes in QA2/CD24 expression in **IFNg** KO mice after *T. cruzi* infection. Thymi from WT or IFNγ KO non-infected control and *T cruzi*-infected mice (9-10 dpi) were obtained as described above. The expression of (A) CD24 and (B) QA2 in SP4 and SP8 thymocytes was analyzed by using flow cytometry. Two-way ANOVA was used for statistical analysis. Data are shown as the mean ± SEM for control versus *T. cruzi*-infected WT and IFNγ KO mice.

Supplementary data to this article can be found online at https://doi.org/10.1016/j.micinf.2024.105337.

References

[1] Boehm T. Thymus development and function. Curr Opin Immunol 2008;20:178–84. https://doi.org/10.1016/j.coi.2008.03.001.

[2] Ciofani M, Zuniga-Pflucker J.C. The thymus as an inductive site for T lymphopoiesis. Annu Rev Cell Dev Biol 2007;23:463–93. https://doi.org/10.1146/annurev.cellbio.23.090506.123547.

[3] Baez N.S, et al. Thymic expression of IL-4 and IL-15 after systemic inflammatory or infectious Th1 disease processes induce the acquisition of "innate" characteristics during CD8+ T cell development. PLoS Pathog 2019;15:e1007456. https://doi.org/10.1371/journal.ppat.1007456.

[4] Morrot A, et al. Chagasic thymic atrophy does not affect negative selection but results in the export of activated CD4+CD8+ T cells in severe forms of human disease. PLoS Negl Trop Dis 2011;5:e1268. https://doi.org/10.1371/journal.pntd.0001268.

[5] Nunes-Alves C, Nobrega C, Behar S.M, Correia-Neves M. Tolerance has its limits: how the thymus copes with infection. Trends Immunol 2013;34:502–10. https://doi.org/10.1016/j.it.2013.06.004.

[6] Hodge D.L, et al. MCP-1/CCR2 interactions direct migration of peripheral B and T lymphocytes to the thymus during acute infectious/inflammatory processes. Eur J Immunol 2012;42:2644–54. https://doi.org/10.1002/eji.201242408.

[7] Barrios B, et al. Abrogation of TNFalpha production during cancer immunotherapy is crucial for suppressing side effects due to the systemic expression of IL-12. PLoS One 2014;9:e90116. https://doi.org/10.1371/journal.pone.0090116.

[8] Rodriguez C.M, et al. Effects of rapamycin in combination with fludarabine on primary chronic lymphocytic leukemia cells. Leuk Lymphoma 2019;60:1299–303. https://doi.org/10.1080/10428194.2018.1529309.

[9] Rodriguez C.M, et al. Intracytoplasmic filamentous inclusions and IGHV rearrangements in a patient with chronic lymphocytic leukemia. Leuk Lymphoma 2018;59:1239–43. https://doi.org/10.1080/10428194.2017.1370549.

[10] Savid-Frontera C, et al. Exploring the immunomodulatory role of virtual memory CD8(+) T cells: role of IFN gamma in tumor growth control. Front Immunol 2022;13:971001. https://doi.org/10.3389/fimmu.2022.971001.

[11] Savid-Frontera C, et al. Safety levels of systemic IL-12 induced by cDNA expression as a cancer therapeutic. Immunotherapy 2022;14:115–33. https://doi.org/10.2217/imt-2021-0080.

[12] Watanabe M, et al. Intradermal delivery of IL-12 naked DNA induces systemic NK cell activation and Th1 response in vivo that is independent of endogenous IL-12 production. J Immunol 1999;163:1943–50.

[13] Rodriguez-Galan M.C, Bream J.H, Farr A, Young H.A. Synergistic effect of IL-2, IL-12, and IL-18 on thymocyte apoptosis and Th1/Th2 cytokine expression. J Immunol 2005;174:2796–804. https://doi.org/10.4049/jimmunol.174.5.2796.

[14] Cardillo F, et al. B cells modulate T cells so as to favour T helper type 1 and CD8+ T-cell responses in the acute phase of Trypanosoma cruzi infection. Immunology 2007;122:584–95. https://doi.org/10.1111/j.1365-2567.2007.02677.x.

[15] Romani L, Puccetti P, Bistoni F. Interleukin-12 in infectious diseases. Clin Microbiol Rev 1997;10:611–36. https://doi.org/10.1128/CMR.10.4.611.

[16] Fink P.J, Hendricks D.W. Post-thymic maturation: young T cells assert their individuality. Nat Rev Immunol 2011;11:544–9. https://doi.org/10.1038/nri3028.

[17] Chau L.A, et al. Thymic re-entry of mature activated T cells and increased negative selection in vascularized allograft recipients. Clin Exp Immunol 2002;127:43–52.

[18] Hardy C.L, Godfrey D.I, Scollay R. The effect of antigen stimulation on the migration of mature T cells from the peripheral lymphoid tissues to the thymus. Dev Immunol 2001;8:123–31. https://doi.org/10.1155/2001/20728.

[19] Shiow L.R, et al. CD69 acts downstream of interferon-alpha/beta to inhibit S1P1 and lymphocyte egress from lymphoid organs. Nature 2006;440:540–4. https://doi.org/10.1038/nature04606.

[20] Gulla S, et al. Role of thymus in health and disease. Int Rev Immunol 2023;42:347–63. https://doi.org/10.1080/08830185.2022.2064461.

[21] de Meis J, et al. Trypanosoma cruzi entrance through systemic or mucosal infection sites differentially modulates regional immune response following acute infection in mice. Front Immunol 2013;4:216. https://doi.org/10.3389/fimmu.2013.00216.

[22] Perez A.R, et al. Thymus atrophy during Trypanosoma cruzi infection is caused by an immuno-endocrine imbalance. Brain Behav Immun 2007;21:890–900. https://doi.org/10.1016/j.bbi.2007.02.004.

[23] Cotta-de-Almeida V, et al. Trypanosoma cruzi infection modulates intrathymic contents of extracellular matrix ligands and receptors and alters thymocyte migration. Eur J Immunol 2003;33:2439–48. https://doi.org/10.1002/eji.200323860.

[24] Mendes-da-Cruz D.A, Silva J.S, Cotta-de-Almeida V, Savino W. Altered thymocyte migration during experimental acute Trypanosoma cruzi infection: combined role of fibronectin and the chemokines CXCL12 and CCL4. Eur J Immunol 2006;36:1486–93. https://doi.org/10.1002/eji.200535629.

[25] Ho Tsong Fang R, Colantonio A.D, Uittenbogaart C.H. The role of the thymus in HIV infection: a 10 year perspective. AIDS 2008;22:171–84. https://doi.org/10.1097/QAD.0b013e3282f2589b.

[26] Nobrega C, et al. Dissemination of mycobacteria to the thymus renders newly generated T cells tolerant to the invading pathogen. J Immunol 2010;184:351–8. https://doi.org/10.4049/jimmunol.0902152.

[27] Francelin C, Paulino L.C, Gameiro J, Verinaud L. Effects of Plasmodium berghei on thymus: high levels of apoptosis and premature egress of CD4(+)CD8(+) thymocytes in experimentally infected mice. Immunobiology 2011;216:1148–54. https://doi.org/10.1016/j.imbio.2011.03.009.

[28] Rafei M, Rouette A, Brochu S, Vanegas J.R, Perreault C. Differential effects of gammac cytokines on postselection differentiation of CD8 thymocytes. Blood 2013;121:107–17. https://doi.org/10.1182/blood-2012-05-433508.

[29] Rafei M, et al. Development and function of innate polyclonal TCRalphabeta+CD8+ thymocytes. J Immunol 2011;187:3133–44. https://doi.org/10.4049/jimmunol.1101097.

[30] Martinez R.J, Hogquist K.A. The role of interferon in the thymus. Curr Opin Immunol 2023;84:102389. https://doi.org/10.1016/j.coi.2023.102389.

[31] Won H.Y, Liman N, Li C, Park J.H. Proinflammatory IFNgamma is produced by but not required for the generation of Eomes(+) thymic innate CD8 T cells. Cells 2023;12. https://doi.org/10.3390/cells12202433.